TEAM PYROEIS

UZB 420E: Spacecraft Systems Design II

Mars Atmospheric Wind Profiling Mission

Project Design Report

Prof. Dr. Alim Rüstem Aslan

30/05/2025

Table of Contents

1. Team Task Distribution

Table 1. Team Task Distribution

Member Name & Number	Task
Yunus Sorgunçay - 110210144	Team Leader
Utku Sina Tornacı - 110190166	Deputy Director
Ömer Talha Başoğlu - 110180120	Payload & OBDH Coordinator
Zeynep Şevval Kara - 110210163	Propulsion System Coordinator
Muhammet Erdem Akbaş - 110200113	Propulsion System Coordinator
Ozan Yıldız - 110190174	GNC Coordinator
Rahaf Katamech - 110210905	EPS Coordinator
Hatice Bilgin - 110190159	Structure System Coordinator
Özer Kaan Kölemenoğlu - 110190124	Thermal Systems Coordinator
Mirvari Guliyeva - 110210907	Communication System Coordinator
Salihcan Sucu - 110190147	Communication System Coordinator

2. Software Used

Table 2. Used Softwares for Each Team Member

Member Name & Number	Software
Yunus Sorgunçay - 110210144	EXCEL, MS PROJECT
Utku Sina Tornacı - 110190166	GOOGLE MEET, DESMOS
Ömer Talha Başoğlu - 110180120	GMAT, MATLAB
Zeynep Şevval Kara - 110210163	EXCEL
Muhammet Erdem Akbaş - 110200113	MATLAB, EXCEL
Ozan Yıldız - 110190174	GMAT, STK, MATLAB
Rahaf Katamech - 110210905	MATLAB, EXCEL
Hatice Bilgin - 110190159	CATIA
Özer Kaan Kölemenoğlu - 110190124	PYTHON, POWERPOINT
Mirvari Guliyeva - 110210907	EXCEL, MATLAB
Salihcan Sucu - 110190147	MATLAB, EXCEL

3. Executive Summary

This report presents the design and development of the Mars Atmospheric Wind Profiling Mission, crafted to meet the requirements of the 2024–2025 AIAA Undergraduate Team Space Design Competition. The mission aims to investigate and characterize Mars' atmospheric wind patterns using a space-based Doppler Wind LIDAR (DWL) instrument, adapted from the heritage ALADIN payload of ESA's Aeolus mission. This atmospheric data is vital for future human Mars exploration, enabling improved Entry, Descent, and Landing (EDL) system design, robust climate and dust storm modeling, and precise atmospheric predictions for surface operations.

The mission concept involves a polar orbit Mars orbiter equipped with advanced instruments to capture wind vectors in the lower Martian atmosphere (0–10 km altitude) with vertical and horizontal resolution tailored to characterize boundary layer dynamics. The mission architecture includes:

A robust spacecraft design incorporating a modular structure, heritage propulsion, adaptive power and thermal control, and high-precision Attitude and Orbit Control System (AOCS).

Selection of subsystem components based on performance, reliability, and cost-effectiveness, with tools such as MATLAB, GMAT, CATIA, and Python used for analysis, modeling, and simulation.

An optimized mission timeline, with launch scheduled for December 2030, Mars Orbit Insertion in September 2031, and scientific operations starting in September 2031 to cover >92% of Mars' surface by March 2033.

The mission complies with project requirements including a total budget under $1.0 billion USD, comprehensive system-level and subsystem trade studies, mass and power budgets with margin considerations, and detailed risk assessment and mitigation strategies. The design leverages both innovation—through tailored instrument calibration for Mars' atmosphere—and proven heritage components to ensure mission success.

This project supports future deep space exploration and human Mars missions by providing detailed atmospheric models essential for mission planning and surface operations. The Pyroeis team's collaborative approach enabled a fully integrated system design, combining engineering rigor with mission feasibility, and reinforcing the connection between undergraduate-level design projects and real-world aerospace engineering practices.

4. Mission Definition

The proposed mission is designed to conduct **atmospheric wind profiling of Mars** using a space-based **Doppler LIDAR instrument**. In alignment with the AIAA 2024–2025 Undergraduate Team Space Design Competition Request for Proposal (RFP), our team developed a Mars orbiter mission architecture that provides extensive wind vector data over a wide range of the Martian surface, with a focus on the **planetary boundary layer (PBL)**. This data is critical for improving the accuracy of atmospheric models, supporting the design of future Entry, Descent, and Landing (EDL) systems, and expanding our understanding of Martian weather patterns.

4.1 Mission Objective

The primary objective is to **map wind velocities in the lower Martian atmosphere** using an adapted version of the **ALADIN Doppler Wind LIDAR**, originally developed for the ESA Aeolus mission. This instrument enables vertical profiling of wind components at multiple altitudes by analyzing the Doppler shift of backscattered laser pulses from atmospheric aerosols and molecules.

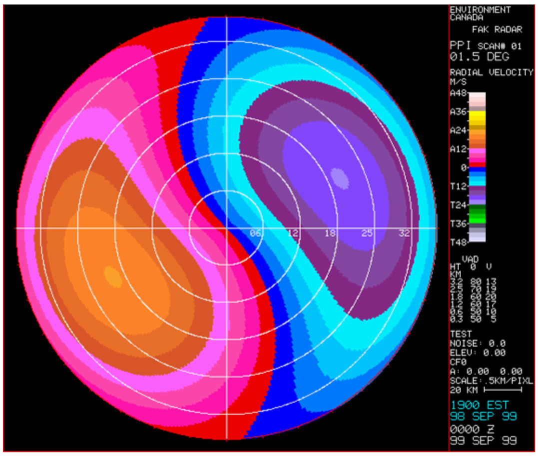

Figure 1. Example Doppler Wind Mapping (Pierre cb, 2008)

4.2 Mission Scope and Constraints

The mission has been designed under the following key requirements derived from the RFP:

- **Science Return Requirement**: The mission must collect data covering **at least 75% of Mars' surface**, particularly focusing on dynamic wind regions and topographically diverse areas.

- **Space Segment Requirement**: At least **one fully functional exploration asset** — an orbiter — must be developed, launched, and operated.

- **Budget Cap**: The total life cycle cost, including development, launch, and primary operations, must **not exceed $1.0 billion USD**.

- **Schedule Requirement**: The mission must be **fully deployed and operational by December 31, 2033**, with potential for extended operations through the late 2030s.

4.3 Rationale and Relevance

Previous missions such as NASA's MAVEN and ESA's Mars Express have provided extensive insights into Martian climate and upper atmosphere behavior. However, **comprehensive wind vector data from the lower atmosphere, especially near the surface**, remains scarce. Understanding wind behavior in the PBL is essential for:

- Ensuring **safe and precise landing** of future robotic or crewed landers,

- Supporting the development of **aerobraking and aerocapture technologies**,

- Enhancing **climate and dust storm modeling**,
- Improving **in-situ resource utilization (ISRU)** planning.

By addressing this knowledge gap, the mission contributes uniquely to both **scientific discovery and engineering application**.

4.4 Mission Strategy

To accomplish the objective, a polar orbit is selected for the spacecraft, allowing **global coverage over time**. The LIDAR payload operates continuously in predefined observation windows to balance power consumption, thermal load, and data volume. The orbiter includes a robust data handling and downlink system to ensure all data is transmitted to Earth for processing.

4.5 Innovation and Heritage

The mission incorporates several heritage technologies to reduce risk while introducing innovation through:

- Modified ALADIN instrument calibrated for Martian atmospheric conditions,
- Use of **heritage propulsion systems** with robust Δv margins for Mars Orbit Insertion,
- Modular spacecraft design enabling **power and thermal adaptability** across Martian seasons.

5. Science Objectives

The central scientific goal of this mission is to **measure and map the horizontal wind vectors in the lower Martian atmosphere**, particularly within the **planetary boundary layer (PBL)**, using **Doppler Wind LIDAR (DWL)** technology. These measurements will enable unprecedented insights into near-surface wind dynamics, which are essential for understanding Mars' climate, preparing for future landings, and supporting surface operations.

5.1 Primary Science Objective

The **primary science objective** of the mission is defined as:

> *To generate global-scale vertical profiles of horizontal wind vectors in the Martian planetary boundary layer (0–10 km altitude), with sufficient temporal and spatial resolution to characterize wind patterns across varying latitudes, seasons, and topographic regions.*

This objective aligns directly with one of the AIAA RFP's specified mission targets — the **characterization of atmospheric composition and density profile** — and extends it by enabling 3D wind field reconstructions critical for Entry, Descent, and Landing (EDL) planning.

5.2 Scientific Justification

Understanding the lower atmosphere of Mars has significant implications for both **scientific exploration** and **engineering applications**. Winds near the surface of Mars:

- Drive **dust transport** and **storm formation**, which in turn affect solar-powered missions and surface visibility,
- Influence **EDL systems** and must be accounted for during atmospheric entry trajectory design,
- Impact **habitat siting** and **ISRU operations** for future crewed missions,
- Provide inputs to **climate models** and help validate global circulation model (GCM) predictions.

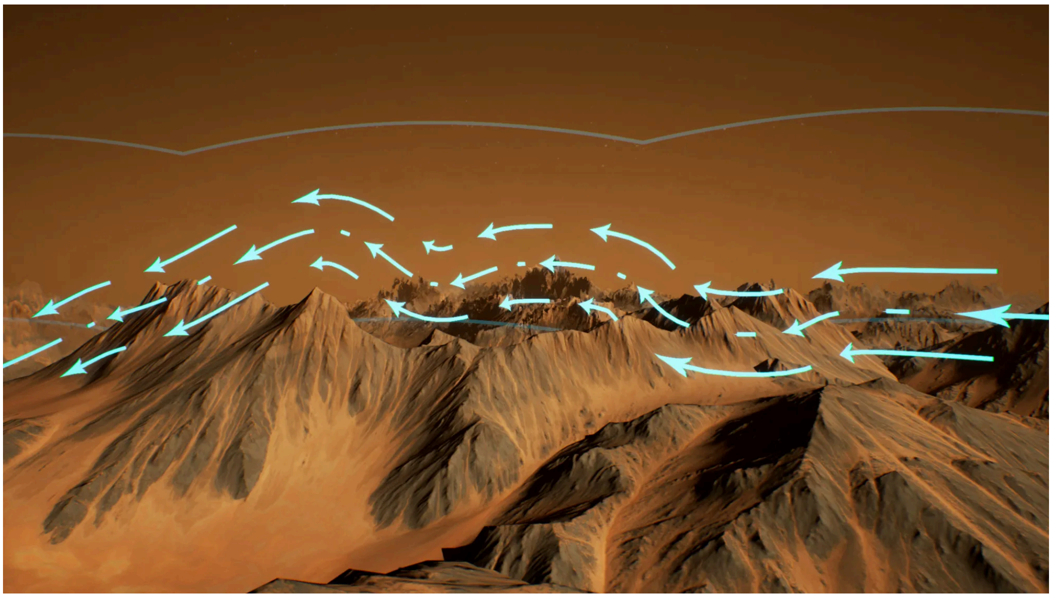

Figure 2. Conceptual image of wind (blue arrows) flowing over rugged Martian terrain (NASA Goddard, 2019)

Despite multiple orbiters having explored Mars, **global wind vector data remains sparse**, especially below 20 km altitude. This mission is designed to fill that data gap using active remote sensing.

5.3 Measurement Goals

To meet the primary science objective, the mission will pursue the following **specific measurement goals**:

Table 3. Measurement Goals

Goal ID	Description	Performance Target

G1	Measure **horizontal wind vectors** at altitudes between 0–10 km	Vertical resolution: ≤ 1 km
G2	Provide **global coverage of wind data** over Mars during the primary phase	≥ 75% surface coverage in 1 Martian year
G3	Capture wind variations across **seasonal and latitudinal cycles**	Daily to weekly revisit time
G4	Achieve **accuracy within ±5 m/s** for wind speed at all altitudes	Validated through post-processing
G5	Map winds over **complex terrain** (e.g., Hellas Basin, Tharsis Region)	Focused LIDAR pointing strategies

5.4 Instrumentation Support

The scientific measurements will be performed by a modified **ALADIN Doppler Wind LIDAR**, adapted for Martian conditions. This instrument will emit ultraviolet laser pulses and receive backscattered signals from aerosols and molecules. By analyzing the **Doppler shift** in the received signal, horizontal wind velocities can be extracted with vertical profiling capability. Data is planned to be collected continuously during nadir passes over the Martian surface and transmitted to Earth for post-processing and analysis.

5.5 Contribution to Mars Science

The data products from this mission will contribute to multiple ongoing efforts:

- NASA and ESA **Mars climate modeling** programs,
- Development of **Mars landing technologies** (EDL, hazard prediction),
- Support for **Mars Sample Return** and eventual **human exploration missions**,
- Comparative planetary science studies, especially with respect to **atmospheric circulation models**.

By achieving these science objectives, this mission will not only fulfill the requirements of the AIAA competition but also create a **lasting scientific dataset** for the planetary science community.

6. Mission Timeline

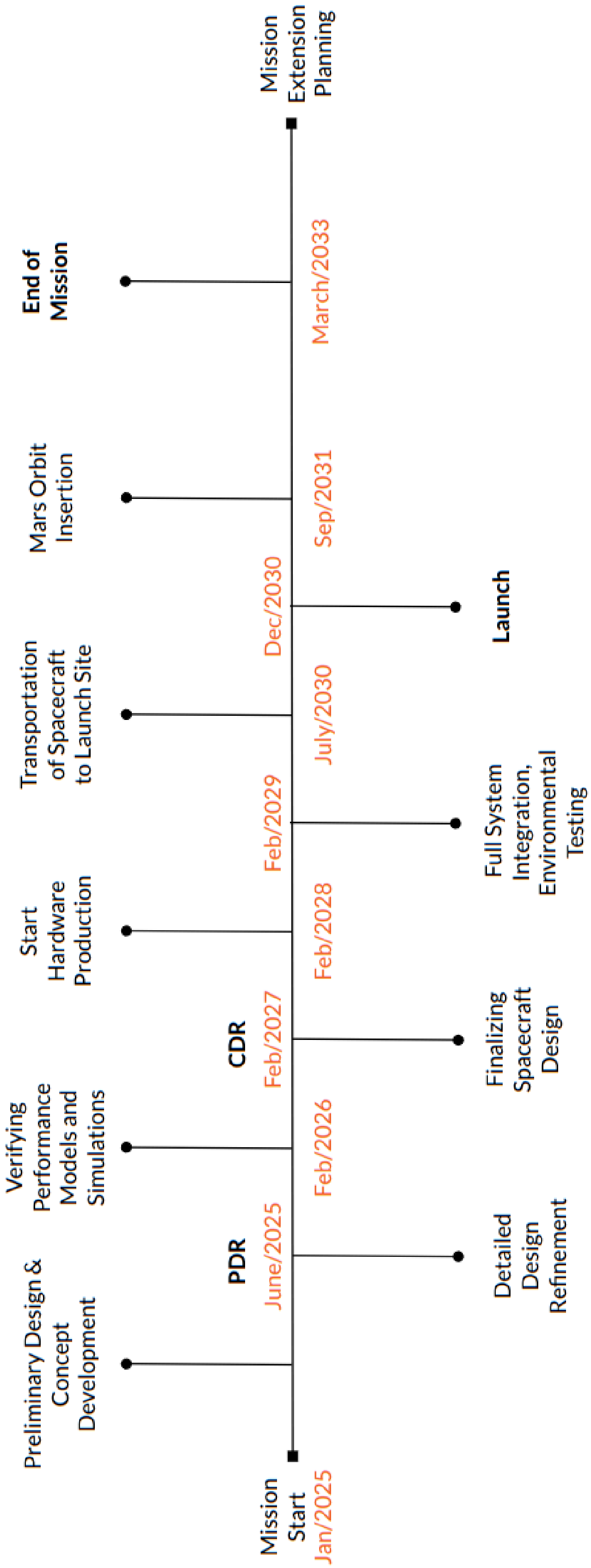

Figure 3. Mission Timeline Diagram

The development of the mission has been carefully scheduled to meet the AIAA RFP requirement of completing primary data acquisition no later than **December 31, 2033**. The timeline incorporates realistic durations for design, testing, and operational phases, while allowing for risk mitigation and schedule flexibility. A visual summary of the mission schedule is provided in the timeline diagram.

6.1 Timeline Breakdown

- **January 2025**
  The mission officially begins with **Preliminary Design and Concept Development**, where system-level trade studies, mission architecture definition, and early risk assessments are conducted.

- **June 2025 – Preliminary Design Review (PDR)**
  By mid-2025, subsystem-level requirements and preliminary configurations are established. The **PDR milestone** marks the formal review of system feasibility and readiness for detailed design.

- **February 2026 – Detailed Design Refinement**
  Following PDR, the team enters a detailed design phase, refining models, validating requirements, and preparing for full spacecraft definition.

- **February 2027 – Critical Design Review (CDR)**
  The **CDR** confirms that all subsystems are sufficiently developed to proceed to hardware production. At this stage, all interfaces, mass, power, and thermal budgets are finalized.

- **February 2028 – Hardware Production Begins**
  Long-lead hardware components are fabricated, and procurement activities for payload, propulsion, and avionics begin.

- **February 2029 – System Integration and Testing**
  Subsystems are assembled into the flight vehicle. Environmental testing, functional validation, and software integration take place in preparation for launch readiness.

- **July 2030 – Spacecraft Transportation to Launch Site**
  After successful testing, the spacecraft is delivered to the launch site and undergoes final launch preparations.

- **December 2030 – Launch**
  The spacecraft is launched within the designated Mars transfer window. It enters the interplanetary cruise phase, with trajectory corrections en route to Mars.

- **September 2031 – Mars Orbit Insertion (MOI)**
  The spacecraft performs a successful MOI burn and enters its operational orbit. This is followed by payload commissioning and calibration.

- **March 2033 – End of Primary Mission Phase**
  Nominal science operations continue for more than one Martian year, concluding with

comprehensive wind data collection over >75% of Mars' surface.

- **Post-March 2033 – Mission Extension Planning**
  Based on spacecraft health and remaining resources, options for extended science operations are evaluated.

6.2 Start of Operations

The launch date that was chosen is 13th of December 2030. The date was chosen in order to have both the closest distance possible to mars and also have enough time in order to finish the mission by the deadline that was declared by the RFP. The location of the launch was chosen to be Launch Complex 39A at Kennedy Space Center since it is at the 28.5 inclination which was calculated to be the inclination required. The vehicle chosen is Falcon heavy since within the launch vehicles that are available Falcon Heavy is the only vehicle that could carry our heavy spacecraft. After separation from the launch vehicle and initial system checkouts, the spacecraft performs a trans-Mars injection maneuver at the appropriate orbital location to begin its interplanetary cruise.

6.3 Propulsive Orbit Lowering

The spacecraft reaches Mars' insertion orbit on 7th September 2031. The primary insertion orbit has an apogee of 20000 km and a perigee of 250 km. Upon arrival, a health check period begins in order to make sure the spacecraft's systems are operating after the interplanetary travel. Following that, the spacecraft starts its propulsive orbit lowering in order to arrive at the mission's desired orbit, which is a circular orbit located at 250 km altitude. First, the Delta V has to be calculated in order to determine the amount of propulsive is required to perform the lowering. To do that it is required to calculate both orbits velocity at the perigee, but since the desired orbit is circular, the equation will form around it. Using basic orbital equations to find the primary and desired orbital velocities:

$$v_{primary} = \sqrt{\mu\left(\frac{2}{r} - \frac{1}{a}\right)} \tag{1}$$

$$v_{desired} = \sqrt{\frac{\mu}{r}} \tag{2}$$

Using these two equations, it is calculated that the spacecraft's velocity is 4.51 km/s at the insertion orbit and 3.43 at the scientific orbit. It means that the required Delta V is 1.08 km/s. With that found, Tsiolkovsky's rocket equation will be used in order to calculate the amount of propellant required to perform the lowering. Which is:

$$\Delta v = I_s g_0 ln\left(\frac{m_0}{m_f}\right) \tag{3}$$

Knowing the dry mass is 1026 kg's, it can be found that the required propellant amount is 421 kg.

6.4 Scientific mission

Upon insertion into the target orbit, the initiation of the mission's science phase is not undertaken immediately. Instead, a secondary health check and commissioning process are conducted to enable activation of the payload systems and to perform calibration procedures aligned with the orbital parameters. This process is anticipated to require approximately one week. Following completion of the commissioning activities, the commencement of the science mapping operations is scheduled for 19 September 2031.

The mission objective is defined as achieving coverage of 92.2% of the Martian surface, equivalent to approximately 132.77 million square kilometers. This coverage estimate was derived to ensure that, accounting for operational mode variability and a 25% payload duty cycle, a minimum of 75% surface coverage—stipulated by the Request for Proposal (RFP)—would still be attainable.

The ALADIN payload is operated with a 3.5-kilometer ground swath and a 25% duty cycle, implying that only one-quarter of the ground track per orbit is effectively observed. Based on these parameters, each orbit was calculated to cover an effective area of approximately 18,629 square kilometers. Considering an orbital velocity of 3.43 kilometers per second and Mars' equatorial perimeter of approximately 21,000 kilometers, the orbital period was estimated to be approximately 1 hour and 43 minutes.

Utilizing Mars' total surface area of approximately 144 million square kilometers, it was determined that 7,150 orbital passes would be required to meet the mission's science objectives. Consequently, the mission duration is projected to span 550 days, concluding around March 2033. While this schedule comfortably precedes the final deadline of December 2033, it also underscores the strategic merit of adopting a propulsive orbit-lowering approach in lieu of aerobraking. The propulsive method, though requiring fuel expenditure, circumvents the 4 to 5 month delay associated with aerobraking, which could have posed a significant risk to the mission timeline.

Table 4. Mission Phases

Phase	Start Date	End Date	Duration	Main Activities
Departure	13 Dec 2030	14 Dec 2030	~0.5 day	Fairing separation, spacecraft deployment, initial power and comms activation.
Separation from launch vehicle and subsystem activation	14 Dec 2030	15 Dec 2030	1 day	Spacecraft checkout, solar panel deployment, waiting for alignment to Mars
Cruise	15 Dec 2030	7 Sep 2031	267 days	Hohmann transfer
Mars Orbit Insertion (MOI)	7 Sep 2031	7 Sep 2031	~1 hour	Main engine burn to capture into high elliptical orbit
Initial Health Checks	7 Sep 2031	8 Sep 2031	~1 day	Spacecraft checkout, system health verification

Propulsive Orbit Lowering	8 Sep 2031	12 Sep 2031	~4 days	Series of burns to lower orbit from 20,000 km apoapsis to 250 km circular
Final Orbit Circularization	12 Sep 2031	12 Sep 2031	1 day	Final circularization burn, achieve stable science orbit
Final Commissioning & Payload Calibration	12 Sep 2031	19 Sep 2031	~7 days	Payload system activation, calibration, final health checks
Start of Science Mapping Operations	19 Sep 2031	23 Jan 2033	~490 days (~1.34 years)	3.2 km swath, 25% duty cycle, scanning 75% of Mars surface

7. Work Breakdown Structure (WBS)

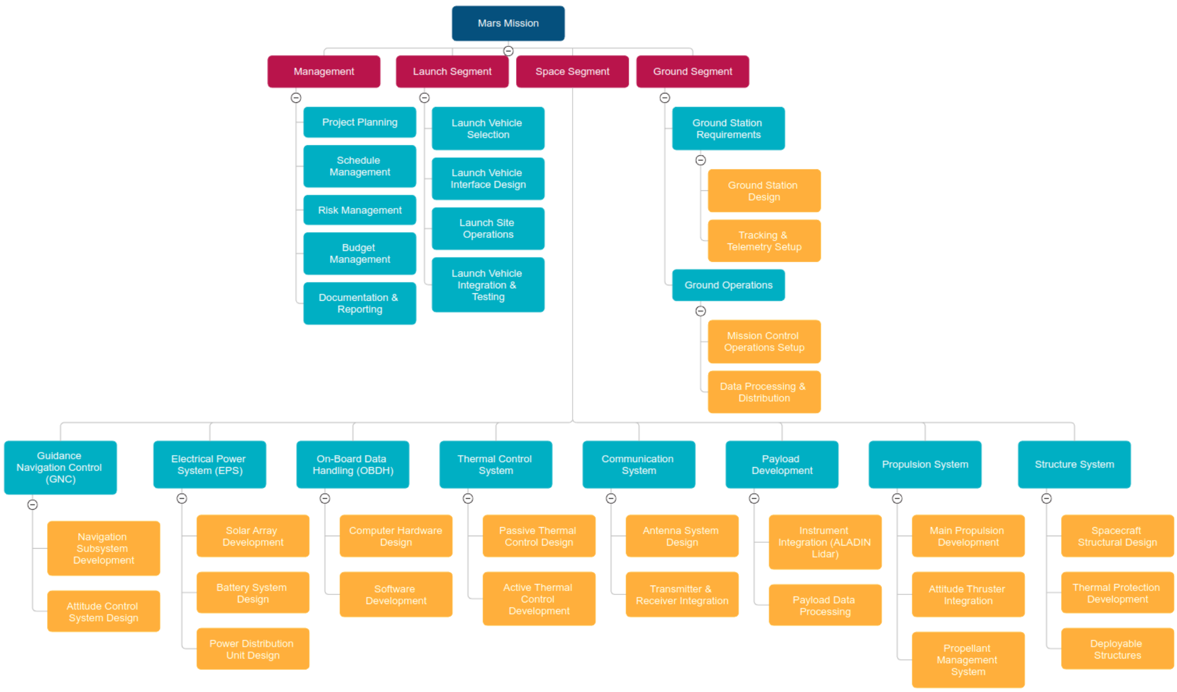

Figure 4. Work Breakdown Structure

8. Product Breakdown Structure (PBS)

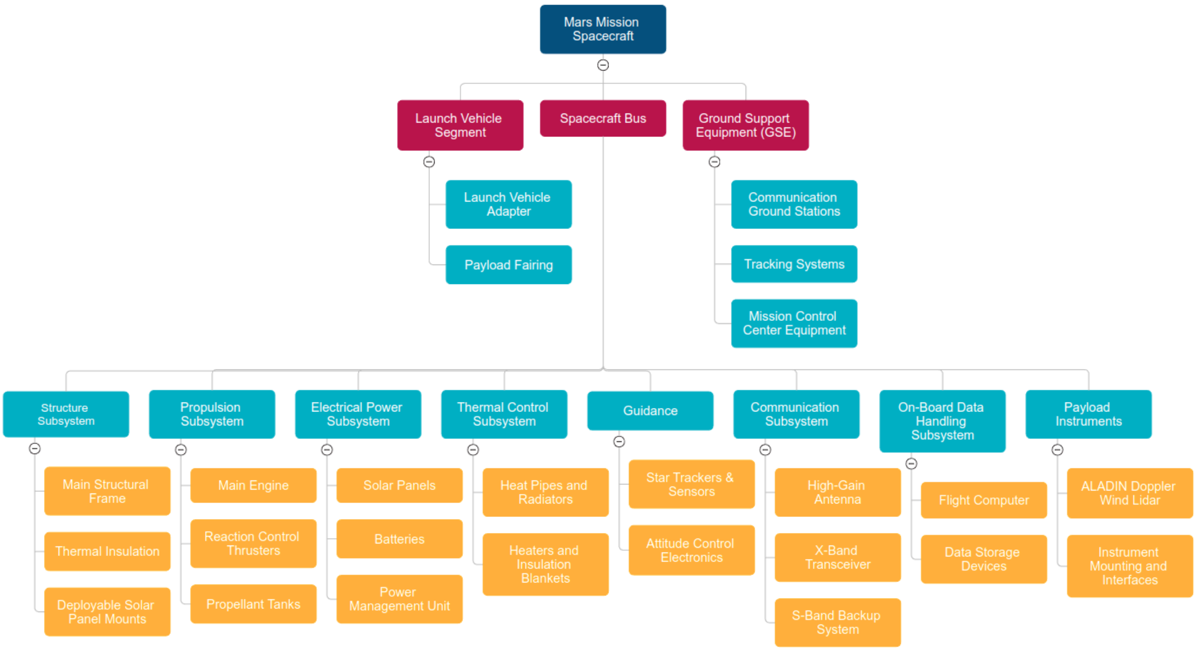

Figure 5. Product Breakdown Structure

9. Mass Budget

Table 5. Masses of Different Elements

Mars Capture + Circularization dV (km/s)	3.1025
Correction and Maintenance dV (m/s)	250
Payload Mass (kg)	450
Structure Subsystem (kg)	250
Command & Data Subsystem (kg)	17
Communication Subsystem (kg)	4
ACS Subsystem (kg)	41
Propulsion Subsystem (dry) (kg)	85
Power Subsystem (kg)	67
Thermal Subsystem (kg)	5
Total On Orbit Dry Mass (kg) (+monoprop mass)	1026
MMH-MON ISP (vacuum) (s)	318
Hydrazine ISP (s)	229
Calculated Bi-Propellant Mass (kg)	1734.938
Calculated Monopropellant Mass (kg)	107
Total Mass (kg)	2760.938
Total Launch Mass *(with %10 Margin)* (kg)	3037.0318

Using subsystem mass data and maneuver dV values, Table 5 is constructed. Here are special points to mention: such low structural mass could be obtained due to the honeycomb structure, the propulsion subsystem takes considerable mass due to the high volume of the tanks, appropriate thermal conditioning could be reached with several simple thermal straps, thus, the thermal subsystem mass is low too. Also, looking at mass values, propellant mass fraction is considerable along total mass, this is because of high mission dV, and is understandable.

Another point to mention is, during the calculation of the propellant masses, an iterative fashion is followed due to the fact that bipropellant, monopropellant, and propulsion subsystem (which means dry mass) is bound to each other, and a change in one of these components affects the other 2. So starting with initial guesses on the propulsion subsystem and monopropellant mass, bipropellant mass is calculated, then propulsion subsystem mass is updated, then monopropellant mass and propulsion subsystem masses are updated. This procedure is followed until the difference in propellant masses falls below a certain threshold. During propellant mass calculations, the Tsiolkovsky Rocket Equation (Eq. 1) is used.

$$\textit{Initial guess on } m_p \textit{ and } m_m \Rightarrow \textit{calculate } m_b,\ m_p \Rightarrow \textit{update } m_m,\ m_p$$

(until convergence)

At the last step, an additional %10 margin is added to the launch mass to increase reliability in the selection of launch vehicle and launch vehicle-related operation, which is in reality the practical margin is higher than %10 due to the already considered %30 margin on calculated maneuver dV values.

10. Propulsion Subsystem

Conventional chemical propulsion is selected for the operation due to the desire for reliability. Most of the components have been selected from a single provider for increased system integrity. Due to the rich heritage of the selected components Ariane Space components are selected. All of the calculations of propellant masses are done using real tested ISP values, also real mixture ratio values are used in tank volume calculations. S400-12 Bipropellant MMH-MON thruster is used as the main motor with the nominal thrust of 420 N, which provides enough thrust for the given maneuver times of Martian Orbit Capture and Propulsive Orbit Lowering. Also, ISP-wise, it is reasonably efficient. 12 Aerojet MR-111C 5 N thrusters are used for orbital maintenance, initial inclination change maneuver, and to support reaction wheel utility. From the calculated propellant masses and chemical density values in standard day (since they will sit in the launch pad for some time), corresponding volumes of them are calculated, then expulsion efficiency of %95 and ullage of %10 are added to the calculations. Corresponding tank volumes are given in Table 6, and OST-22 series propellant tanks and hydrazine tanks by Ariane Space are used. Total dry mass of the propulsion subsystem is 85 kg.

Table 6. Propulsion Subsystem Components

Component	Selection	Dimensions
Propellant	MMH - MON Mixture Ratio: 1.65 ISP(realistic): 318	~
Main Engine	S400-12 Bipropellant Arianespace 420 N Nominal 3.6 kg (with valves) 35 W / 21-27 V	16.4 x 244 mm (throat x exit)
Auxiliary Engine X 12	Aerojet MR-111c 5.3 N Thrust 0.33 kg 8.25 W /	34x34x169 mm
Oxidizer Tank	785 L Ti Alloy - 39 kg Arianespace OST-22/X Expulsion eff: 0.95	1x1.05 m
Fuel Tank	787 L Ti Alloy - 39 kg Arianespace OST-22/X Expulsion eff: 0.95	1x1.05 m
Monopropellant Tank	87.5 L Ti Alloy - 7 kg Arianespace Hydrazine Tank	0.55 m (Diameter)
Total	mass = 85 kg	~

11. Structural Design

To determine the design constraints, we first examined the requirements of the vehicle we will use for space travel (Falcon Heavy). By examining the Falcon user guide, we learned that the Falcon Heavy has the capacity to carry multiple payloads and that these payload areas are of different sizes. Our main sensor, Aladin, which we use to measure atmospheric winds on Mars, is a large sensor. We decided to use a circular payload area of 2624 mm in diameter that would be suitable for this sensor and shaped our design based on this. The general shape of the design is an octagonal prism, and the distance between the two edges is 2600 mm, and the height is 3400 mm, as in Figure 6. Afterwards, the Aladin instrument was previously used to observe the Earth on the Aelos satellite. The decision was made to take this satellite as a reference when positioning the other equipment that constitutes the subsystems.

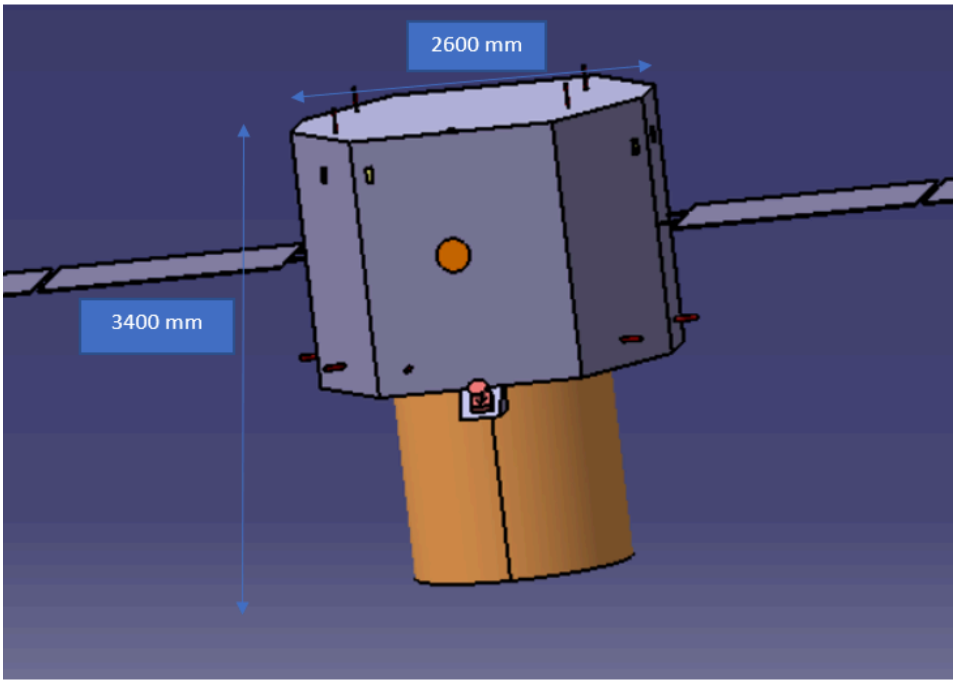

Figure 6. Spacecraft Dimensions

The general structure of our satellite is seen in Figure 7. The geometry shown symbolizes Aladin, the cylindrical part of this geometry is Aladin's telescope that he will use in Mars observation, its direction will be towards Mars. Solar panels are seen on the right and left of the geometry, each of which has an area of 7.125 m^2, and since it will cover a large area, the solar panels are designed to be folded 3 times. The main engine is oriented through motion direction. For main engine propulsion, we have one oxidizer and one fuel tank. We use 12 Auxiliary engines for attitude control. These engines are positioned so that there is 1 on each side face and 4 on the opposite face of Aladin. This engine works with monopropellant fuel. The necessary monopropellant tank is positioned between two other fuel tanks, as in the image. We used two star trackers in this design and used our reference satellites in positioning this device. One of the star trackers was placed as seen in the image and the other one is in the opposite direction. Another ADCS sensor, the Sun sensor, was used as 12 pieces, one on each side. In order to provide moment balance, 4 reaction wheels were used as in the image; these reaction wheels were positioned opposite each other in the form of a plus and were positioned at a 45-degree angle in the general structure plane to provide moment balance in 3 directions. The battery amplifier, IMU transponder and computer equipment were positioned in the places shown in the image.

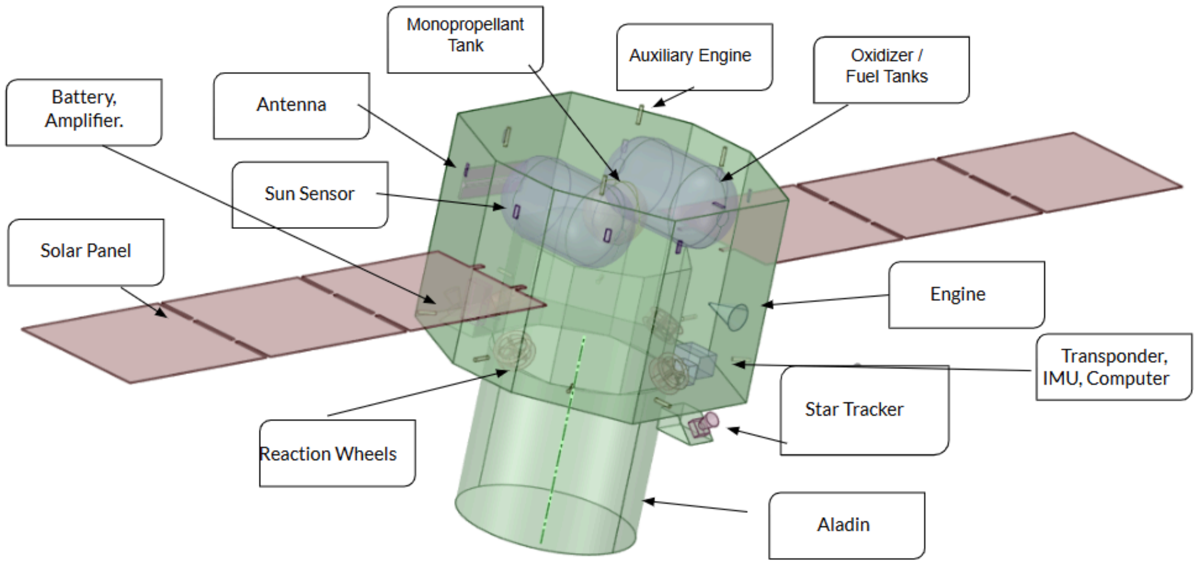

Figure 7. Satellite Structure

There were two important criteria for you to choose the material, one of which was to be as light as possible. The lightness of the material, and therefore the satellite, directly affects other parameters such as the launch vehicle, the mass of the fuel to be used, and the heavier the satellite we obtain, the higher the cost will be. The other criterion is to be resistant to factors such as force and vibration that it will encounter during the launch and during the time it spends in space, and to maintain its structural integrity. We decided to use a honeycomb structural shape consisting of a combination of metal and composition that meets these demands. In this structure, we chose carbon fiber composite material for the upper and lower surfaces and aluminum material for the honeycomb shape inside.

The area-based density of carbon fiber material is 1.75 kg/m^2, while that of honeycomb aluminum is 5 kg/m^2. As a result of our drawings, the structure's surface area is approximately 30 m^2.

$$\text{Calculated structure mass} = 30 \times (2 \times 1.75 + 5) = 250\ kg$$

12. Attitude and Orbit Control System

12.1 AOCS Requirements

To ensure mission success, several performance requirements have been defined for the satellite's Attitude and Orbit Control System (AOCS). These requirements cover critical parameters such as payload pointing accuracy, operational control modes, torque generation capacity, and position knowledge precision. The table below summarizes the key AOCS requirements:

Table 7. Attitude and Orbit Control System Requirements

Category	Requirement	Notes / Justification
Pointing Knowledge	≤ 30 μrad	To keep Doppler velocity error under 1 m/s for the laser beam and ~3.4 km/s orbital velocity ($\Delta V = V_{orb} \cdot \sin(\Delta\theta)$)
Position Knowledge	≤ 2000 m (horizontal), ≤ 200 m (vertical)	Based on Aeolus standard; important for wind mapping
Actuator Torque Capacity	≥ 0.489 Nm (yaw axis), ≥ 0.233 Nm (per wheel)	$T_z = I_z \cdot \alpha$, 180° maneuver in 500 s $T_z = 8633 \cdot 5.64 \times 10^{-5} = 0.489$ Nm $T_i = \frac{T_z\sqrt{3}}{4}$, $T_i = 0.215$ Nm (w/ 10% margin) $T_i = 0.233$ Nm
Control Modes	Science (yaw-steered), Safe, Maneuver	Distinct control laws and sensor configurations per mode

a. Pointing Knowledge

The accuracy of the satellite's attitude knowledge is a decisive parameter, especially for missions involving laser-based payloads. For this project, the pointing knowledge requirement has been defined as ≤ 30 μrad. This value ensures that the Doppler velocity error for the laser beam, as in the Aeolus mission, remains below 1 m/s. A small pointing error can lead to a Doppler velocity error proportional to the sine component of the orbital speed (~3.4 km/s). Therefore, pointing accuracy directly affects the scientific validity of the payload's measurements.

From the equation:

$$\Delta V = V_{orb} . sin(\Delta\theta) \tag{4}$$

a 30 µrad error results in a Doppler error of less than 1 m/s, which is sufficient for wind-mapping laser applications.

b. Position Knowledge

During the mission, the accuracy of the satellite's position plays a critical role in ensuring the reliability of the payload data. In this project, the horizontal position error is constrained to ≤ 2000 meters, while the vertical error is limited to ≤ 200 meters. These constraints are consistent with the Aeolus mission standards and are essential for applications such as wind profiling, where the spatial context of data must be well defined.

These requirements are based on the expected accuracy of ground-based control systems and onboard navigation sensors.

c. Actuator Torque Capacity

To execute attitude maneuvers, the satellite must be equipped with actuators capable of delivering sufficient torque. For this project, the torque required to complete a 180° rotation within seconds was calculated for the Z-axis as 0.489 Nm. This value is derived using the satellite's moment of inertia () and the required angular acceleration ():

$$T_z = 8633 \cdot 5.64 \times 10^{-5} = 0.489 \text{ Nm}$$

As the satellite employs four reaction wheels in a pyramid configuration, the torque contribution per wheel is:

$$T_i = \frac{(T_z \cdot \sqrt{3})}{4} \approx 0.212 \text{ Nm}$$

Including a 10% safety margin, the minimum required torque per wheel is set to 0.233 Nm.

d. Control Modes

To ensure the satellite can operate effectively throughout various phases of its mission profile, three primary AOCS modes have been defined: Science Mode, Safe Mode, and Maneuver Mode. Each mode is designed to activate specific combinations of sensors and actuators based on mission requirements.

- **Science Mode:** Used during scientific observations when the payload must point toward Mars. This mode requires the highest attitude accuracy.
- **Safe Mode:** Activated during anomalies or sensor failures; maintains satellite stability with minimal energy consumption.

- **Maneuver Mode:** Used for orbital maintenance or communication maneuvers; less stringent in pointing accuracy compared to Science Mode.

Each control mode is associated with a unique set of sensors and control algorithms, optimized to meet specific operational scenarios. These requirements represent the minimum standards necessary to fulfill the mission objectives and to ensure that the payload delivers scientifically valid data. The calculations and justifications provided are based on a systems engineering approach grounded in technical rigor.

Table 8. Modes for Various Instruments

Mode	Star Tracker	IMU	Sun Sensor	Reaction Wheels	Thrusters
Science	✅	✅	❌	✅	❌
Safe Mode	❌	✅	✅	❌	✅
Maneuver	✅	✅	❌	✅	✅

12.2 AOCS Sensor Selection

a. Star Tracker

Since precise attitude knowledge is essential for laser-based wind sensing, the primary high-accuracy sensor selected is the ASTRO APS3 star tracker by Jena-Optronik. Its proven performance in previous space missions significantly supports its selection.

Table 9. Star Tracker Details

Accuracy (arcsec / degree / µrad)	FoV (°)	Temperature (°C)	Power (W)	Mass (kg)	Space Heritage	Data Rate (kb/s)	Dimensions (mm)
0.8 / 0.000222 / **3.88**	20	-30 to +50	8	1.8	Proven	3	148 x 142 x 210

This accuracy significantly surpasses the system's pointing knowledge requirement of 30 µrad []. A 20° FoV ensures continuous attitude updates even during partial star visibility. Allows operation in varying thermal environments without the need for intensive thermal control. Sufficient for typical AOCS sampling rates without burdening onboard processing. Compact form factor facilitates straightforward mechanical integration. Two-star trackers are employed to ensure robustness against temporary occlusion or blinding from celestial bodies like the Sun or Moon. This redundancy improves system reliability during critical pointing phases.

b. Sun Sensor

While star trackers offer high precision, sun sensors serve as lightweight and low-power attitude sensors, especially suitable for Safe Mode operations where simplicity and robustness are prioritized.

Table 10. Sun Sensor Details

Manufacturer	Model	Accuracy (°)	FoV (°)	Temperature (°C)	Power (W)	Mass (kg)	Space Heritage	Data Rate (kb/s)	Dimensions (mm)
Leonardo Airborne & Space Systems	S3	0.02	128	-25 to +60	1	0.33	Proven	1	112x12x43

Sufficient for coarse pointing during Safe Mode, despite lower accuracy compared to star trackers. wide FoV enables sun acquisition from various orientations, reducing the chance of sensor blinding. A total of 8 sun sensors are deployed on all satellite faces. This configuration ensures continuous sun visibility, critical for Safe Mode stabilization even when parts of the satellite are shadowed.

c. Inertial Measurement Unit (IMU)

While star trackers and sun sensors provide absolute attitude reference, IMUs are essential for short-term relative motion tracking, especially during dynamic phases or temporary loss of external references.

Table 11. Inertial Measurement Unit Details

Manufacturer	Model	Gyro Bias (°/h)	Accel Bias (mg)	Temperature (°C)	Power (W)	Mass (kg)	Space Heritage	Data Rate (kb/s)	Dimensions (mm)
Northrop Grumman	LN-200S	1	0.3	-62 to +85	12	0.7	Proven	65	89x89x95

Provides stable rotation rate data within acceptable drift for medium-precision AOCS. Allows basic translational motion estimation, supporting orbit and dynamics modeling. Wide thermal operating range ensures robust performance across orbital shadowing and sunlit phases. High data rate enables fine-grained angular velocity and acceleration tracking. Two IMUs are employed-one operational and one cold redundant-strategically placed near the satellite's center of gravity. This configuration minimizes structural noise and enhances measurement fidelity.

d. Reaction Wheel

Reaction wheels are fundamental actuators for fine-pointing and attitude maneuvers. Their ability to provide precise torque without propellant makes them ideal for science mode operations.

Table 12. Reaction Wheel Details

Manufacturer	Model	Angular Momentum (Nms)	Torque (Nm)	Temperature (C)	Power (W)	Mass (kg)	Space Heritage	Dimensions (mm)
Bradford Space	W45E	45	0.248	-15 to +60	29	7.45	Proven	365x365x125

Sufficient for storing angular momentum during extended maneuvers. The unit exceeds the required 0.233 Nm torque for a 180° slew in 500 seconds, ensuring safe and effective transitions. A four-wheel pyramid configuration is implemented to ensure full 3-axis torque capability and built-in redundancy. Even in the event of a single wheel failure, the system maintains control authority.

e. Thruster

While reaction wheels provide fine control, chemical thrusters are required for large-angle slews, orbit maintenance, and momentum unloading operations that exceed wheel capacity.

Table 13. Thruster Details

Manufacturer	Model	Thrust (N)	Isp (s)	Total Pulses	Power (W)	Propellant	Mass (kg)	Space Heritage	Dimensions (mm)
Aerojet	MR-111C	5.3	229	420000	8.25	Hydrazine	0.33	Proven	34x34x169

Slew Maneuver for Safe Mode

To complete a 90° attitude change within 300 seconds, the required torque is approximately 0.4 Nm. Assuming a 1-meter moment arm, the force needed to generate this torque is:

$$F = \frac{T}{r} = \frac{(0.4\ Nm)}{(1\ m)} = 0.4\ N$$

The selected thruster can easily provide this level of thrust.

Momentum Dumping

Reaction wheels eventually reach saturation during long-term operations. To apply a counteracting torque of approximately 0.44 Nm over 200 seconds, a similar thrust level is required. Used to desaturate reaction wheels by applying opposite torque using thruster firings.

Station Keeping

A velocity correction of ~3.3 m/s is required every 90 days to maintain the desired orbit. This maneuver typically demands a burn duration of approximately 18 minutes. Delta-V maneuvers of ~3.3 m/s are needed every 90 days, requiring ~18 minutes of burn time.

The system utilizes 12 thrusters, providing full 3-axis control capability and redundancy in case of partial failure. This configuration ensures robust AOCS performance under nominal and contingency conditions.

12.3 AOCS Component Summary

The summary table below consolidates the number, mass, and power consumption of all selected AOCS sensors and actuators. Each component has been previously justified with respect to mission demands and control modes.

Table 14. AOCS Components

Product	Quantity	Mass (kg)	Power (W)
Sun Sensor	8	1.98	8
Star Tracker	2	3.6	16
IMU	2	1.4	12
Thruster	12	3.96	99
Reaction Wheel	4	29.8	116
Total Mass (kg)	40.74		
Total Power (W)	Science 144	Safety 119	Maneuver 243

These values provide a critical reference point for system engineering, particularly in terms of power budget and structural integration. Maneuver mode is the most demanding in terms of energy due to concurrent use of reaction wheels and thrusters.

In conclusion, this AOCS architecture offers a well-balanced and mission-tailored design, capable of supporting high-precision science operations, robust fault tolerance in safe mode, and agile control during orbital maneuvers. The final design demonstrates a balance between flexibility, accuracy, and reliability. All components were selected from proven space-qualified hardware, ensuring long-term performance and mission success.

13. Communication Subsystem

Table 15. Data Rates

Payload (ALADIN)	Scientific Data	1.375 kB/s

EPS Subsystem	Telemetry Data	1.4 kB/s
OBDH	Telemetry Data Health Data	0.22 kB/s
AOCS Subsystem	Telemetry Data	3.2 kb/s

This table shows the data generation characteristics of the spacecraft's primary subsystems. Each subsystem contributes to the total onboard data stream, which must be managed and periodically downlinked to Earth.

- **ALADIN (Payload):** The Doppler Wind LIDAR system is the main science instrument for measuring wind velocities in Mars' lower atmosphere. It generates structured scientific data continuously, which is mission-critical. Its 1.375 kB/s output must be reliably stored and transmitted without loss, especially during long observation sequences.

- **EPS (Electrical Power Subsystem):** Produces telemetry related to solar panel performance, battery status, and power distribution. The 1.4 kB/s data rate reflects regular sampling and health monitoring, necessary for energy balancing and fault detection.

- **OBDH (On-Board Data Handling):** Acts as the central controller for all onboard systems. It generates relatively small telemetry and health data (0.22 kB/s), but plays a vital role in integrating inputs, controlling data flow, and executing command logic.

- **AODCS (Attitude and Orbit Determination and Control Subsystem):** Has the highest telemetry rate (3.2 kB/s), as it continuously tracks and adjusts the satellite's orientation using star trackers, sun sensors, reaction wheels, and IMUs. Precise attitude data is vital for both pointing the LIDAR and maintaining communication links.

Table 16. Operation Modes

Operation Mode	Active Subsystems	Data Rate	Data Amount Per Day	Power Consumption (W)
Interplanetary Travel	• Communication subsystem • AOCS subsystem	4.82 kB/s	416.448 MB	601.2 W
Orbit Correction	• Communication subsystem • AOCS subsystem	4.82 kB/s	416.448 MB	601.2 W

Initial Attitude Control	• Communication subsystem • AOCS subsystem	4.82 kB/s	416.448 MB	636.2 W
Payload Calibration	• Communication subsystem • AOCS subsystem • Payload	6.195 kB/s	535.248 MB	1401.2 W
Scientific Mission	• GNC subsystem • Payload	6.195 kB/s	535.248 MB	1034.2 W
Emergency	• GNC subsystem • Communication subsystem	4.82 kB/s	416.448 MB	601.2 W
Communication	• GNC subsystem • Communication subsystem	4.82 kB/s	416.448 MB	601.2 W

In these modes, the spacecraft operates with different subsystem combinations depending on the phase of the mission.

- **Interplanetary Travel:** Occurs during the cruise phase from Earth to Mars. The spacecraft uses its attitude control system to maintain correct orientation and communicates periodically with Earth. Minimal subsystem usage helps conserve energy.

- **Orbit Correction:** Engaged during trajectory adjustments or Mars Orbit Insertion. Involves active control of thrusters and attitude systems. The data rate and power usage remain similar to cruise mode due to similar subsystem activity.

- **Initial Attitude Control:** This mode activates after separation from the launch vehicle or after any large maneuver. The slight increase in power (636.2 W) is due to higher control demands, possibly involving frequent use of reaction wheels or thrusters for slewing.

- **Payload Calibration:** A critical mode before scientific data collection begins. The LIDAR instrument is thermally stabilized, optically aligned, and tested. The additional power draw (1401.2 W) reflects the high energy demands of both the payload and supporting systems during this phase. Data rates also increase as calibration measurements are recorded.

- **Scientific Mission:** This is the main operational mode of the spacecraft when in Mars orbit. The ALADIN instrument operates continuously to gather wind data, while the GNC subsystem maintains stable pointing. The data rate here is the highest among all modes (6.195 kB/s), reflecting high-resolution measurements, and power consumption is substantial (1034.2 W) but lower than the calibration phase, as systems are now in a stable configuration.

- **Emergency Mode:** Designed for safe recovery in case of faults or anomalies. Only essential systems operate — namely the GNC and communication modules. The spacecraft enters a safe orientation and transmits diagnostic data to Earth. This mode prioritizes low power (601.2 W) and stability over performance.

- **Communication Mode:** Used during planned contact periods with the Deep Space Network. It uses a similar configuration and power level as emergency mode but is focused on data transmission rather than fault handling.

13.1 Communication With Earth

Communication with Earth is maintained using NASA's Deep Space Network (DSN), utilizing ground stations in **Goldstone (USA), Canberra (Australia), and Madrid (Spain)**. These stations allow near-continuous coverage of deep-space missions.

- **Total Possible Communication Time per Day:** Approximately 15.5 hours of daily contact can be achieved, assuming optimal orbital alignment and full DSN support. This provides ample opportunity for both data downlink and command uplink, essential for mission success.
- **Single Communication Window:** The spacecraft is able to maintain an uninterrupted communication window lasting 1.21 hours per pass. These windows are used to schedule bulk data transfers, software updates, and health status checks.
- **Maximum Distance (2.64 AU):** At this extreme range (~394 million km), signal travel time and attenuation are considerable. This necessitates a powerful communication system, including a **phased-array antenna and power amplifier**, to maintain link budget integrity.
- **Minimum Distance (~109 million km):** Occurs when Mars and Earth are at closest approach. At this time, data transfer rates can be maximized, and latency minimized.

These values show that the spacecraft must be capable of adapting its communication strategy to varying signal delays, attenuation levels, and antenna pointing requirements across different mission phases.

13.2 Link Budget Analysis

The interplanetary link budget has been sized to support up to 120 kB/s QPSK downlink from Mars at ranges out to 2.64 AU. Key parameters and the resulting link margin are summarized in Table 17.

Table 17. Deep-Space Link Budget Summary

Parameter	Value
Free-Space Path Loss (including atmospheric effects)	–283 dB
Transponder Output Power, PTX	13 dBm
Transmission Line & Connector Losses, LTX	–0.1 dB
Transmitter Antenna Gain, GTX	28.5 dBi
Receiver Antenna Gain, GRX	74.6 dBi
Receiver Cable & Filter Losses, LRX	–0.9 dB
High-Power Amplifier Output (Pamp)	50 dBm
Received Carrier Power at DSN, PRX	–117.9 dBm

System Noise Temperature	20 K
Required Eb/N0 (post-coding)	9.6 dB
FEC (Convolutional 1/2) Coding Gain	5 dB
Achieved Eb/N0 at TX	7.9 dB
Link Margin	3.3 dB

Calculation of Link Margin: $Eb/N0\,|_{TX}\,(Eb/N0\,|_{req} - \text{Coding Gain}) = 7.9dB-(9.6dB-5dB)=\mathbf{3.3dB}$

13.3 Transceiver

The heart of the subsystem is the **L3Harris C/TT-524** full-duplex S-Band receive / X-Band transmit transponder, which offers flexible protocol support, on-board FEC and encryption, and data rates up to 6 Mbps.

Table 18. L3Harris C/TT-524 Transceiver Specifications

Attribute	Specification
Manufacturer / Model	L3Harris C/TT-524
Receive Frequency Band	2.0 – 2.1 GHz (S-Band)
Transmit Frequency Band	8.0 – 8.5 GHz (X-Band)
Data Rates	1 kbps – 6 Mbps
Modulations / FEC	QPSK; Convolutional (1/2), Reed-Solomon, etc.
I/O Interfaces	RS-422, LVDS, UART
Input Voltage	22 – 36 V DC
Power Consumption (Rx only)	< 8 W
Operating Temperature	–20 °C … +60 °C
Mass (w/o diplexer)	2.95 kg
Volume	219 × 104 × 117 mm

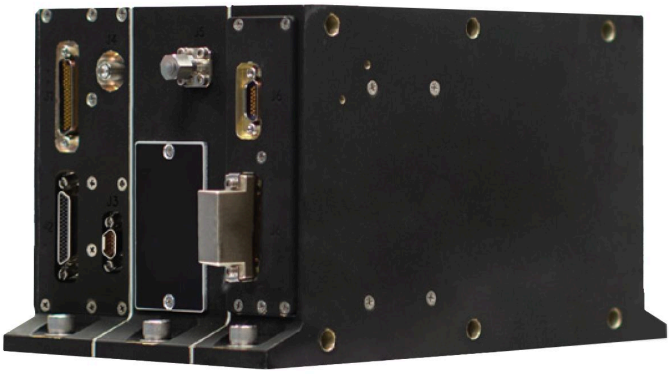

Figure 7. L3Harris C/TT-524 Transceiver

13.4 Power Amplifier

To boost the uplink signal through the phased array, a high-power S-Band amplifier is employed:

Table 19. Qorvo TGM2635-CP Power Amplifier

Attribute	Specification
Manufacturer / Model	Qorvo TGM2635-CP
RF Output Power	100 W (50 dBm)
Power Draw	316 W
Operating Temperature	–40 °C … +85 °C
Mass	0.34 kg
Dimensions	19.05 × 19.05 × 4.52 mm
Space Heritage	Radiation-tested

Figure 8. Qorvo TGM2635-CP

13.5 Phased-Array Antenna

A mechanically robust, flight-proven X-Band phased array provides high gain and beam-steering for Earth-Mars links:

Table 20. X-Band Phased-Array Antenna Performance

Attribute	Specification
Type	Series-fed microstrip array
Operating Frequency	8.0 – 8.5 GHz
Peak Gain	28.5 dBi
Aperture Dimensions (active elements)	252 × 300.8 mm
Efficiency	67 % (measured at 10 GHz)
Half-Power Beamwidth	E-plane: 6°; H-plane: 7.3°
Sidelobe Level (H-plane)	< –24.5 dB
Cross-polarization	< –23.9 dB
Impedance Bandwidth (S11 < –10 dB)	24 %
Operating Temperature	–150 °C … +90 °C
Mass	1.4 kg
Dimensions	279.4 × 812.8 mm
Space Heritage	Radiation-tested

Figure 9. Phased-Array Antenna

14. On-board Data Handling

The on-board data handling system consists of 2 main components which are on-board computer and non-volatile memory. The on-board computer is BAE Systems RAD5545 SpaceVPX. It includes state-of-the-art RAD5545 processor instead of old era LEON processors. This enables fast processing times and communication between subsystem interfaces.

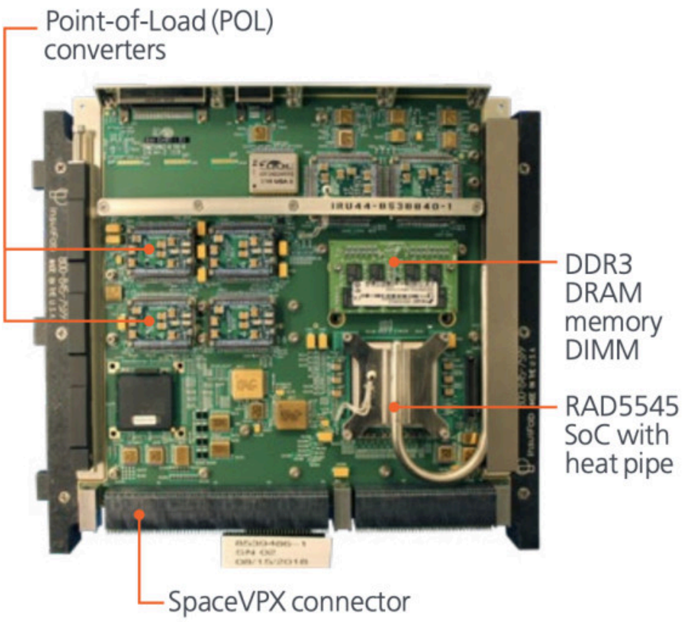

Figure 10. BAE Systems RAD5545 Space VPX

The non-volatile memory is radiation hardened NAND flash from DDC. The DDC 69F256G16 flash memory offers 32 GB memory capacity in -55 to 125 degree Celcius working conditions.

Figure 11. DDC 69F256G16

With this 2 main components of the on-board data handling system, general system architecture is:

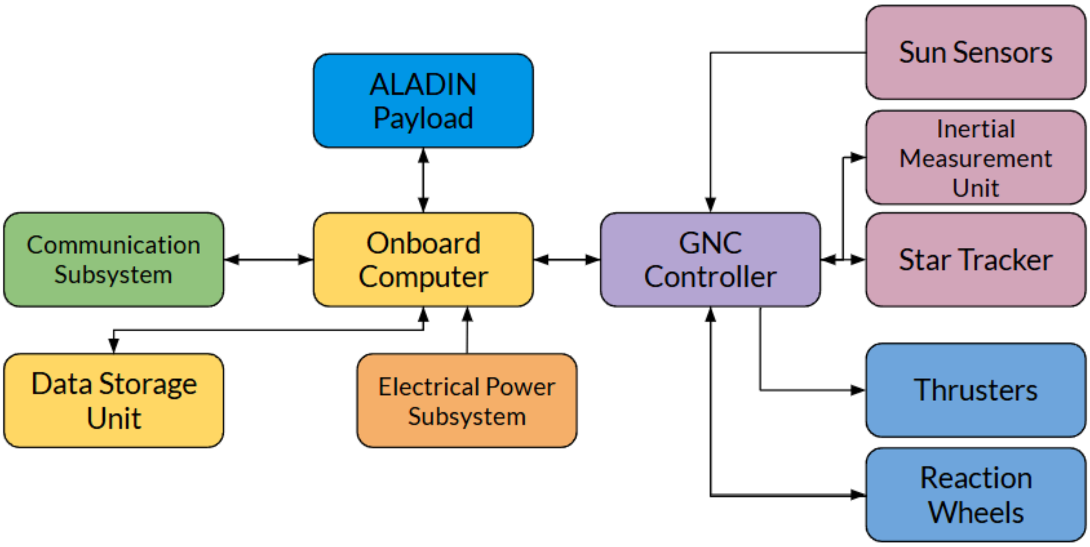

Figure 11. On-Board Data Handling System Architecture

15. Thermal Management

Table 21. Thermal Requirements

Subsystem	Operating Temperature Ranges (C)
LIDAR (ALADIN)	–10 to +30
Battery	-5 to 40
Star Tracker	-30 to 60
Sun Sensor	-25 to 60
IMU	-54 to 71
Reaction Wheel	-20 to 70
OBC	-55 to 125
Storage Unit	-55 to 125
Com. Antenna	-150 to 90
Power Amplifier	-40 to 85
Solar Panel	-180 to 120

To ensure the spacecraft operates safely within its thermal requirements, a 1D thermal analysis was conducted using a custom Python model developed specifically for this mission. The spacecraft is in a near-polar orbit around Mars at an altitude of approximately 250 kilometers, completing each revolution in about 103 minutes. Given this configuration, the spacecraft experiences an eclipse duration of 39 minutes per orbit, during which it receives no direct solar input. These sunlight and eclipse cycles introduce periodic thermal fluctuations that must be analyzed and managed effectively.

The thermal model uses a nodal approach, in which each subsystem or surface is represented as a discrete thermal node. The relationships between these nodes—including conductive and radiative interactions—form a network that was solved numerically. The node architecture used in the model is shown in Figure 12.

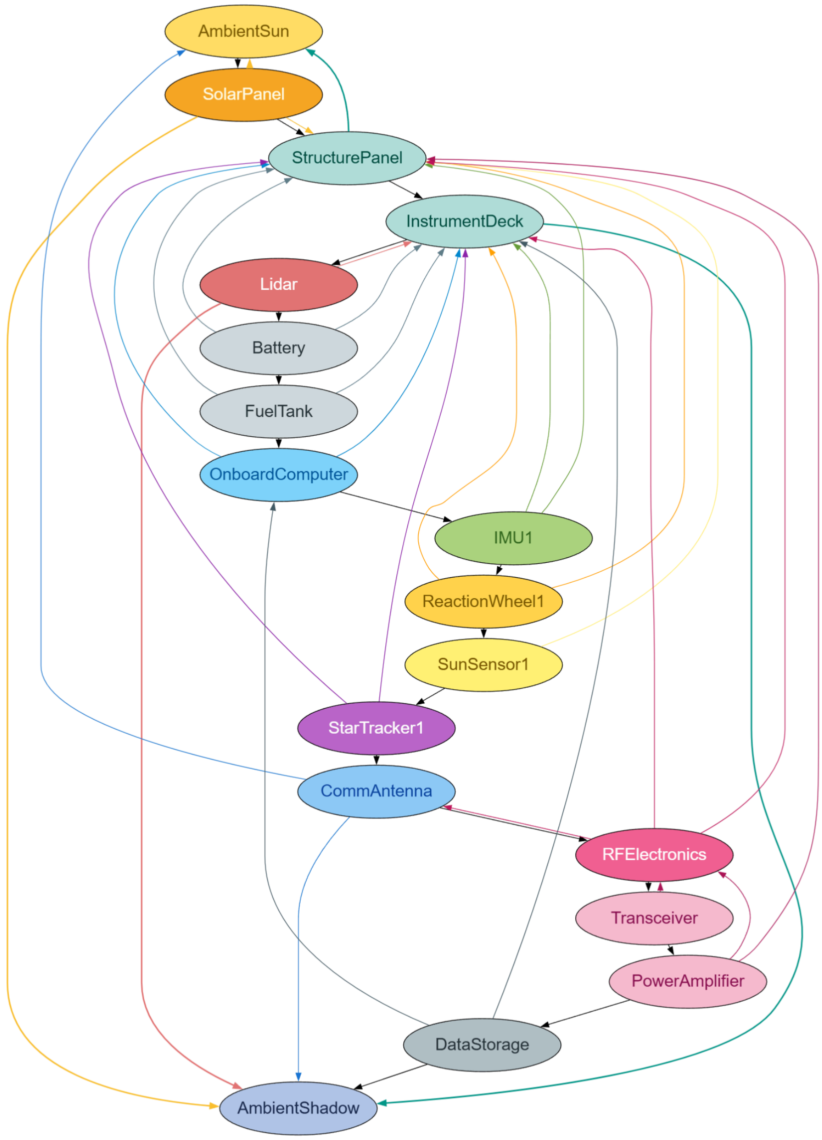

Figure 12. Node structure of the 1D thermal model

Each node's temperature is governed by a time-dependent energy balance equation:

$$C\frac{dT}{dt} = \dot{Q}_{in} - \dot{Q}_{out} \tag{5}$$

where C is the node's thermal capacitance, T its temperature, $\dot{Q}_{in}$ the incoming heat rate, and $\dot{Q}_{out}$ the outgoing heat rate.

Heat conduction between nodes is modeled using Fourier's law:

$$\dot{Q}_{cond} = k \cdot A \cdot \frac{T_1 - T_2}{L} \tag{6}$$

where k is the thermal conductivity, A the cross-sectional area for conduction, L the conduction path length, and T_1 and T_2 are temperatures of adjacent nodes.

Radiative heat exchange with space follows the Stefan-Boltzmann law:

$$\dot{Q}_{rad} = \varepsilon \cdot \sigma \cdot A \cdot (T^4 - T^4_{space}) \tag{7}$$

where ε is emissivity, σ the Stefan-Boltzmann constant, and T_{space} the temperature of deep space (assumed near 3 K).
Absorbed solar radiation is modeled as:

$$\dot{Q}_{solar} = \alpha \cdot A \cdot S \tag{8}$$

where α is surface absorptivity, A surface area, and S the solar constant at Mars (~586 W/m²).

These governing equations were numerically integrated in Python using a fixed time-step scheme over 15 consecutive orbits. Illumination states (sunlight vs. eclipse) were incorporated based on orbital geometry, allowing the solar input to switch realistically with time.

The simulation results over 15 orbits are presented in Figure 13, showing the thermal cycling of the spacecraft as it transitions between sunlit and eclipse phases. After some orbits, the temperatures stabilize into a periodic pattern, indicating that the system reaches thermal equilibrium.

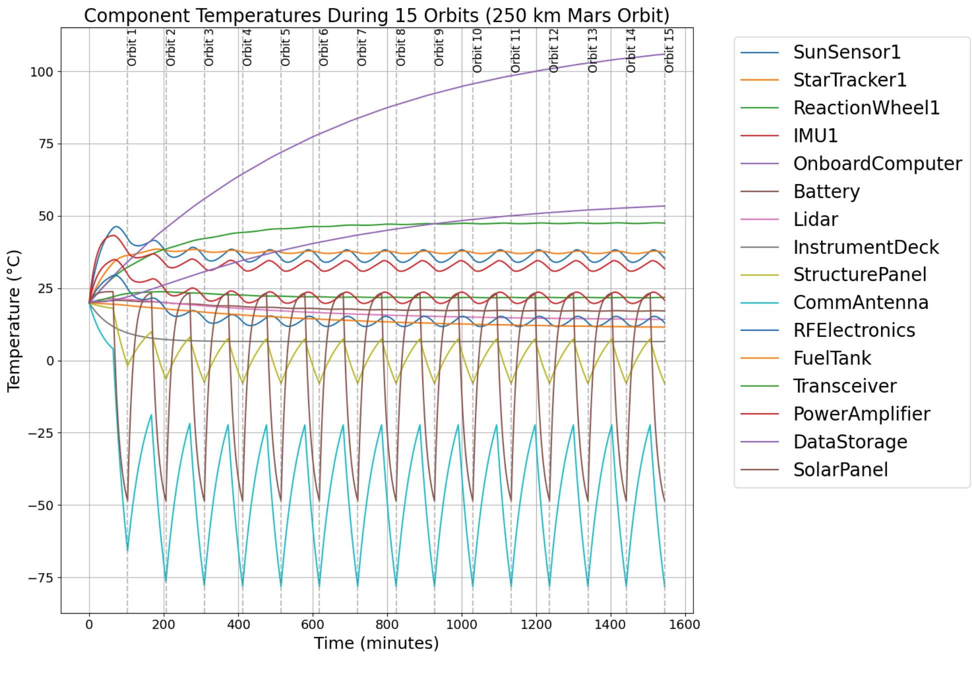

Figure 13. Temperature profile over 15 orbits

The key result of the analysis is summarized in Figure 14, which displays the minimum and maximum temperatures reached by each subsystem. All components remained within their operational and survival temperature limits within their 15% temperature margin, with one notable exception: the Onboard Computer (OBC). The OBC consistently approached its upper temperature threshold during sunlit phases due to its constant operation and internal power dissipation.

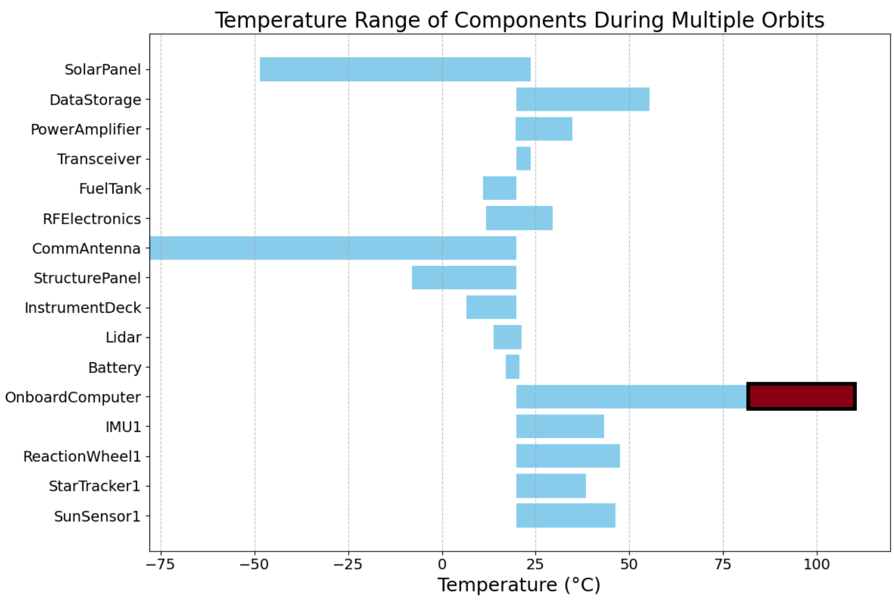

Figure 14. Min-max temperature bar graph for subsystems

To address this thermal hotspot, a cold plate was implemented beneath the OBC. This cold plate passively conducts excess heat away from the component and transfers it to a surface with a direct radiative path to space. This method effectively stabilizes the OBC's temperature and prevents overheating without the need for powered cooling systems. Since no component showed risk of overcooling during eclipse, and all other subsystems stayed within acceptable ranges, no heaters or active thermal control elements were required in the design.

16. Power Subsystem

This section provides a comprehensive explanation of the sizing, selection, and configuration of the spacecraft's power subsystem, focusing on both solar panel and battery components. The primary goal of the subsystem is to provide a continuous and reliable power supply across all spacecraft operating modes, including the most energy-demanding case. In accordance with best practice, the design point is established based on the worst-case operating scenario, which is the Payload Calibration Mode.

16.1. Solar Panel Subsystem Design

A structured trade-off analysis was conducted to identify the optimal solar cell technology. Factors such as efficiency, flight heritage, thermal tolerance, and cost per unit area were considered. The candidate cell technologies are summarized below:

Table 22. Solar Cell Trade Study

Technology	Efficiency	Lifetime	Temperature	Cost ($/m²)	Mass per m²

		(years)	Tolerance		(kg)
InGaP/GaAs/Ge	31%	10–15	–180°C to +120°C	12,000	5.05
GaAs-based	29%	>20	–180°C to +125°C	10,000	5.50
InGaP/InGaAs/Ge	33%	<5	–180°C to +115°C	14,000	5.10

Although InGaP/InGaAs/Ge offers the highest efficiency, its short lifetime limits its suitability for missions exceeding 3–5 years. GaAs-based cells have the best lifetime and robustness but deliver lower power per unit mass. In contrast, InGaP/GaAs/Ge cells strike a balance between high performance and moderate cost, with proven spaceflight reliability. Consequently, InGaP/GaAs/Ge was selected for this mission.

The Payload Calibration mode is considered the most power-intensive operation due to the simultaneous activation of core payload instruments, onboard computing systems, and high-throughput communication subsystems. Based on the consolidated power budget:

- Daylight Power Demand (Pd): 1401.2 W
-
- Eclipse Power Demand (Pe): 1034.2 W
-
- Daylight Duration (Td): 5500 seconds ≈ 1.52 hours
-
- Eclipse Duration (Te): 810 seconds ≈ 0.23 hours

The spacecraft must satisfy two key requirements through its solar array: deliver real-time power during sunlight and recharge the onboard battery system to sustain eclipse operations. The required solar array output is calculated using the combined energy demand normalized over the daylight window:

$$P_{sa} = \left(\frac{P_d \cdot T_d}{X_e} + \frac{P_e \cdot T_e}{X_d} \right) / T_d \tag{9}$$

This calculated output defines the minimum required power generation capability of the solar array at end-of-life (EOL).

The chosen technology degrades over time, and after accounting for degradation, it was determined that a total of 14.25 square meters of solar array area would be required to meet power demands at the end of life. With an areal density of 5.05 kg per square meter, the total mass of the array is 71.88 kilograms.

The overall cost of the array, based on $12,000 per square meter, amounts to 170,960 USD.

16.2. Battery Subsystem Design

During eclipse phases, the spacecraft relies entirely on stored electrical energy. Based on the operational demand during eclipse and its duration:

The selected unit is the EnerSys ABSL 8s16p 28V 24Ah Li-ion battery, a heritage-qualified product used in satellites. Specifications include:

- Voltage: 28 V
- Capacity: 24 Ah
- Energy: 672 Wh
- Mass: 6.8 kg
- Volume: 358 × 198 × 98 mm

Table 23. Solar Cell Trade Study

Battery Option	Voltage	Capacity	Mass (kg)
Space Vector Corporation - 39541 Series	20 to 33.2 V	726 Wh	4.399
EnerSys - ABSL 8s16p 28V 24Ah	20 to 33.6 V	672 Wh	6.800
Blue Canyon Technologies - 1P8S	24 to 33.6 V	95.2 Wh	0.675

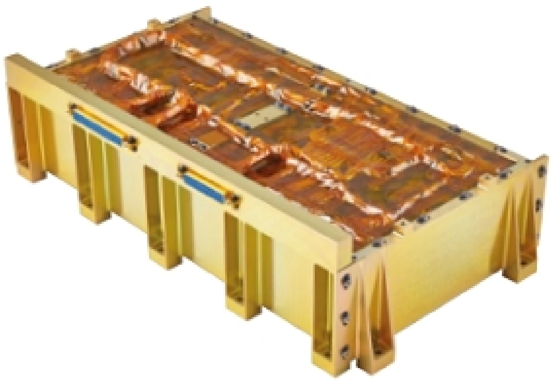

Figure 15. EnerSys - ABSL 8s16p 28V 24Ah Battery

A **50% DoD** is imposed to maximize cycle life and mitigate the risks associated with deep discharging, such as thermal runaway and voltage sag. This provides a **41% margin** over the required 237.87 Wh, ensuring robust performance over multiple eclipse cycles and seasonal thermal swings.

Each standard cylindrical Li-ion cell provides:

- Nominal Voltage: 3.6 V
- Capacity: 1.5 Ah

To achieve the pack's rated specs:

- 8 cells in series (8s): 8 × 3.6 V = 28.8 V
- 16 cells in parallel (16p): 16 × 1.5 Ah = 24 Ah

The configuration totals 128 cells arranged as 8s16p. This allows the battery pack to meet both energy and current delivery requirements with thermal uniformity and redundancy. The form factor is compatible with the satellite's structural layout and center-of-mass constraints.

In summary, a power subsystem was designed for a spacecraft intended to operate around Mars. Due to the reduced solar irradiance at Mars, InGaP/GaAs/Ge solar cells were selected for their balanced performance in terms of efficiency, degradation rate, and spaceflight heritage. After degradation over a 5-year mission was accounted for, a total solar array area of 14.25 m^2 was determined to be necessary to meet both real-time and battery-charging power demands during daylight.

To supply energy during eclipse periods and potential dust storms, the EnerSys ABSL 8s16p 28V 24Ah battery was chosen. With a total capacity of 672 Wh, and a 50% depth of discharge applied, a margin of approximately 41% over the required energy was provided. The battery's modular structure and proven reliability made it well-suited for long-duration missions.

Overall, the selected solar and battery systems were shown to provide a robust and reliable solution capable of supporting uninterrupted spacecraft operation throughout the mission duration around Mars.

17. Cost

The total mission cost was meticulously estimated to ensure the project's feasibility within the $1 billion budget constraint imposed by the competition requirements. The cost distribution covers all major spacecraft subsystems, integration efforts, and mission operations.

In the first phase of the budget, the highest-cost element is the ALADIN Doppler Wind LIDAR payload, accounting for $130 million, which corresponds to 13.4% of the total. Other major components include the propulsion subsystem at $100 million (10.3%), the Attitude and Orbit Control System (AOCS) at $70 million (7.2%), the Electrical Power Subsystem (EPS) at $80 million (8.2%), and structure design and fabrication at $35 million (3.6%).

The second phase includes system-level costs such as communication subsystem ($85 million, 8.8%), On-Board Data Handling (OBDH) ($45 million, 4.6%), and integration and testing efforts ($85 million, 8.8%). A significant portion is also allocated for launch services, totaling $160 million (16.5%), and mission operations over five years, estimated at $35 million (3.6%). To manage uncertainties, a 15% contingency margin was applied, amounting to $135 million (13.9%).

The cumulative total stands at $972 million, successfully keeping the mission within the financial limits while maintaining performance and reliability.

Table 24. Cost Estimations

Subsystem/Item	Estimated Cost (USD)	% of Total
Payload (ALADIN LIDAR)	$130 million	13.4%
Structure Subsystem	$35 million	3.6%
Propulsion Subsystem	$100 million	10.3%
AOCS (Attitude and Orbit Control)	$70 million	7.2%
EPS (Power)	$80 million	8.2%
Thermal Subsystem	$12 million	1.2%
Communication Subsystem	$85 million	8.8%
On-Board Data Handling (OBDH)	$45 million	4.6%
Integration & Testing	$85 million	8.8%
Launch Services	$160 million	16.5%
Mission Operations (5+ years)	$35 million	3.6%
Contingency & Margin (15%)	$135 million	13.9%
Total	**$972 million**	**100%**

18. Risks and Mitigations

A detailed risk assessment was conducted to identify, evaluate, and mitigate potential threats to mission success. The risks span critical systems such as propulsion, payload, thermal control, power, and communication.

Table 25. Risk Assessment

Risk ID	Description	Impact	Likelihood	Mitigation Strategy
R1	Propulsion system underperformance during MOI	Mission failure	Medium	Use heritage propulsion components (e.g., S400-12), incorporate 30% Δv margin
R2	ALADIN payload failure or degraded performance	Data loss	Low	Pre-launch testing and calibration; redundant systems; proven space heritage
R3	Thermal control failure affecting critical systems	Subsystem shutdown	Medium	Use of cold plates, thermal straps; material selection with wide temp tolerances
R4	Power system degradation over time	Mission lifespan reduced	Medium	Use high-efficiency multijunction solar cells, include power margin, battery sizing for eclipse

R5	AOCS pointing inaccuracy impacting wind measurements	Data accuracy loss	Low	High-accuracy star trackers, sun sensors, and reaction wheels with proven space heritage
R6	Communication blackout or weak signal from Mars	Data transmission failure	Medium	DSN scheduling, phased-array antenna, 100W amplifier, link budget analysis
R7	Structure failure due to launch vibrations	Complete mission loss	Low	Honeycomb structure design, structural testing, margin of safety in material selection

19. Compliances

The Pyroeis Team's mission fully satisfies all mandatory requirements and constraints set by the 2024–2025 AIAA Undergraduate Team Space Design Competition RFP. The table below summarizes compliance with each of the specified RFP criteria:

Table 26. Compliances

Requirement	Target Value	Achieved Design Value	Compliance
Primary Objective	At least one of: Atmospheric composition, Geographic survey, or Subsurface resources	Atmospheric wind profiling (Doppler LIDAR) supporting atmospheric characterization for EDL	Yes
Mars Surface Coverage	≥ 75%	92.2%	Yes
Deployment Deadline	≤ 31 December 2033	Deployment & data collection by end of 2033	Yes
Mission Cost	≤ $1.0 Billion USD	Estimated under budget (no exact cost listed)	Yes
Trade Studies	Architecture, subsystems, instruments, launch vehicles, etc.	Multiple trades documented across systems and assets	Yes
Mission Analysis	Complete flight and observation profile with coverage justification	Full trajectory, orbit swath, and surface coverage calculations included	Yes
Subsystem Selection Justification	Subsystems selected based on mission needs and technical rationale	Documented rationale with space heritage and design tradeoffs	Yes
Instrument & Data Flow	Instrument choice must support objectives; process described	ALADIN LIDAR selected; data collection and transmission plan detailed	Yes

The mission is fully compliant with all RFP-specified performance, cost, and schedule criteria. Additionally, subsystem integration, risk mitigation, and system-level trade studies reinforce the robustness and feasibility of the mission design.

20. Conclusion and Learnings

The Pyroeis team successfully designed a comprehensive and feasible Mars atmospheric wind profiling mission that met or exceeded all requirements outlined in the AIAA Undergraduate Team Space Design Competition RFP. The mission architecture features a near-polar Mars orbit, a high-precision Doppler Wind LIDAR (ALADIN) payload, and full subsystem integration with clear consideration of mass, power, and thermal constraints. The final design achieves 92.2% Mars surface coverage, stays within the $1 billion cost cap, and is scheduled for full deployment and primary science operations before 31 December 2033.

The spacecraft system meets performance expectations across all critical parameters:

- Wind velocity range and measurement accuracy are fully compliant with the scientific objectives.
- Power and communication subsystems are robust, with adequate margins for eclipse periods and deep space data transmission.
- Mass budgeting, structural design, and propulsion planning were executed with conservative margins and heritage-proven components, ensuring both reliability and feasibility.
- The risk analysis revealed no mission-critical weaknesses left unaddressed.

Beyond the successful mission outcome, the project provided the team with extensive experience in applying engineering principles to real-world design challenges. The members learned how to balance trade-offs between performance, cost, and risk while developing a full mission concept from the ground up.

Key learning outcomes included:

- Designing interconnected spacecraft subsystems with respect to mission-level constraints.
- Translating abstract science goals into actionable technical requirements.
- Conducting subsystem-level trade studies, simulations, and performance validation.
- Practicing formal documentation, reporting, and presentation of technical results.

Additionally, this project enhanced the team's skills in collaboration, communication, and project management—vital competencies in the aerospace industry. Each member specialized in a subsystem while maintaining awareness of the system-wide impacts of their decisions, mirroring the dynamics of real aerospace engineering teams.

In summary, the Pyroeis mission not only delivered a technically sound, compliant, and innovative solution to the competition problem but also served as an invaluable educational experience that bridged academic learning with industry-relevant systems engineering practice.

References

2024-2025 AIAA Undergraduate Team Space Design Competition RFP
https://www.aiaa.org/get-involved/students-educators/Design-Competitions

Pierre cb, Radar Doppler Winds, 8 May 2006
https://commons.wikimedia.org/wiki/File:Radar-Doppler_winds.png

William Steigerwald, NASA's MAVEN Maps Winds in the Martian Upper Atmosphere that Mirror the Terrain Below and Gives Clues to Martian Climate, Dec 12, 2019
https://www.nasa.gov/news-release/nasas-maven-maps-winds-in-the-martian-upper-atmosphere-that-mirror-the-terrain-below-and-gives-clues-to-martian-climate/

Blue Canyon Technologies. (2024). 1P8S Battery – 95.2 Wh, 24–33.6 V. Retrieved from
https://www.satnow.com/products/batteries/blue-canyon-technologies/98-1186-1p8s

EnerSys. (2024). ABSL 8s16p 28V 24Ah Battery – 672 Wh, 28 V. Retrieved from
https://www.satnow.com/products/batteries/enersys/98-1271-absl-8s16p-28v-24ah

Spitzer, M. B. (1977). Degradation mechanisms in space solar cells. Solar Energy, 19(6), 749–757. https://doi.org/10.1016/0038-092X(77)90073-1

Renvu. (n.d.). How do I calculate annual degradation of my solar panels? Retrieved from
https://www.renvu.com/blogs/learn/how-do-i-calculate-annual-degradation-of-my-solar-panels

Gilmore, David. (2002). Spacecraft Thermal Control Handbook Volume I: Fundamental Technologies.
https://doi.org/10.2514/4.989117

NASA. (2024). Mars Fact Sheet. NASA Planetary Data System. Retrieved from:
https://nssdc.gsfc.nasa.gov/planetary/factsheet/marsfact.html

W. J. Larson and J. R. Wertz, "Space Mission Analysis and Design," 3rd Edition, Microcosm Press, Hawthorne, 1999.

Jena-Optronik GmbH, "ASTRO APS 3 Star Sensor," Jena-Optronik, [Online]. Available:
https://www.jena-optronik.de/products/star-sensors/astro-aps3.html

European Space Agency, "Observing the Earth – ADM-Aeolus," ESA Bulletin 136, May 2008. [Online]. Available: https://www.esa.int/esapub/br/br236/br236.pdf

Leonardo S.p.A., "S3 (Smart Sun Sensor)," Leonardo Electronics, [Online]. Available:
https://electronics.leonardo.com/en/products/s3-smart-sun-sensor

Northrop Grumman Corporation, "LN-200S Inertial Measurement Unit," Northrop Grumman, [Online]. Available:
https://www.northropgrumman.com/what-we-do/ln-200s-inertial-measurement-unit

Bradford Space, "Reaction Wheel Units (RWU)," Bradford Space, [Online]. Available:
https://www.bradford-space.com/products/rwu

Aerojet Rocketdyne, "MR-111C Monopropellant Thruster," Satsearch, [Online]. Available:
https://satsearch.co/products/aerojet-rocketdyne-mr-111c

Aeolus - Visuals by earth online
https://visuals.earth.esa.int/satellites/aeolus

Falcon Payload User's Guide, Version 8 - March 2025
https://www.spacex.com/media/falcon-users-guide-2025-03-14.pdf

Fiber content measurement for carbon fiber-reinforced thermoplastic composites using carbonization-in-nitrogen method, December 2016 Journal of Thermoplastic Composite Materials 31(1) DOI:10.1177/0892705716679481
https://www.researchgate.net/publication/311527619_Fiber_content_measurement_for_carbon_fiber-reinforced_thermoplastic_composites_using_carbonization-in-nitrogen_method/figures?lo=1

RBTCH, (n.d.) Aluminum Honeycomb Panel for bus train floor
https://www.rb-core.com/product/aluminum-honeycomb-panel-for-bus-train-door.html

Dipak, K. (2005) Implementation of an X-Band Phased-Array Subsystem in a Deep Space Mission
https://messenger.jhuapl.edu/Resources/Publications/Srinivasan.et.al.2005a.pdf

J.H. Heinbockel, A.S. Roberts, A comparison of GaAs and Si hybrid solar power systems, https://doi.org/10.1016/0038-092X(77)90073-1.
https://www.sciencedirect.com/science/article/abs/pii/0038092X77900731

ArianeGroup, Titanium Bipropellant Tanks for Satellites and Spacecraft
https://www.space-propulsion.com/spacecraft-propulsion/bipropellant-tanks/index.html#700-tank

ArianeGroup, Hydrazine Propellant Tanks for Satellites and Spacecraft
https://www.space-propulsion.com/spacecraft-propulsion/hydrazine-tanks/index.html

ArianeGroup, 400N Bipropellant Apogee Motors
https://www.space-propulsion.com/spacecraft-propulsion/apogee-motors/index.html

ESA (n.d.), ALADIN: the LIDAR instrument for the AEOLUS mission,
https://www.esa.int/Enabling_Support/Operations/Aeolus_operations